Indian Journal of Chemistry
Vol. 62, December 2023, pp. 1289-1297
DOI: 10.56042/ijc.v62i12.5843

Sulpha drugs based heterochelates: Synthesis, spectroscopic, thermal and *in vitro* biological studies

Darshan Jani*[a] & Maulik Raja[b]

[a] Noble Science College, Noble University, Bhesan Road, Bamangam, Junagadh 362 310, Gujarat, India
[b] Department of Chemistry, Atmiya University, Rajkot 360 005, Gujarat, India
E-mail: darshan.jani@ngivbt.edu.in, darshanjani09@gmail.com, raja_maulik96@ymail.com

Received 27 September 2023; accepted (revised) 24 November 2023

In the current study, dapsone and different 4-acyl pyrazolone derivatives have been used to synthesise various Cu(II) and Ni(II) based heterochelates. Elemental analysis, ^{1}H NMR, IR, and mass spectroscopy have been utilized to check the structure of the tetra dentate DPL1 to DPL5 ligands, and FAB mass spectroscopy as well as temperature investigations (TGA/DTG and DSC) have been utilized to approve the structure of the Cu(II) and Ni(II) heterochelates. All the synthesized compounds have been examined for their *in vitro* biological study against two Gram +ve (*Bacillus cereus*, *Bacillus megaterium*) and two Gram –ve (*Escherichia coli*, *Enterobacter aerogene*) microorganisms as well as their MIC against two Gram +ve (*Bacillus subtilis*, *Staphylococcus aureus*) and two Gram –ve (*Escherichia coli*, *Serratia marcescens*) microorganisms. The outcomes demonstrate the tremendous promise and importance of novel bis-pyrazolone heterochelates based on dapsone for further study.

Keywords: Sulpha drugs, Bis pyrazolone, *In vitro* biological activity, Thermal study, Transition metal heterochelates

Because of their simplicity in production, stability, flexibility and potent bioactivity, complexes based on pyrazolone and its four acyl derivatives have received a lot of interest in recent years[1]. According to studies, compounds of 4-acyl pyrazolone Schiff base derivatives exhibit a wide variety of biological activities, including cytotoxicity, DNA binding activity, antibacterial and antimalarial properties and antitumor properties[2-8]. Therefore, a significant scientific task still exists in the creation and production of new 4-acyl pyrazolone-based metal complexes[9]. Due to the numerous coordination atoms and diverse coordination modes, 4-acyl pyrazolone Schiff base derivatives also have the ability to create various complexes[10,11].In addition to being a significant family of organic molecules, pyrazolone-5 derivatives are also of significant scientific and practical importance in the fields of biology, investigative uses, catalysis, dyes and mining metallurgy[12-16]. Due to the numerous electron-rich supporter centres, they also have the ability to create various kinds of coordination compounds[17,18]. In the meantime, considerable research has been done on the creation of novel bis-pyrazolone-based chelating ligands[19-23]. Studies on compounds based on bis-pyrazolone have shown that they have powerful fluorescence characteristics[24,25] as well as some *in vitro* antitumor and high herbicidal action[26]. As a result, we created a set of four bis-pyrazolone compounds based on acyl pyrazolone (DPLn). The two donor citations in this novel chelating ligand are positioned at 5,5′/-OH groups. They can create different kinds of metal compounds because there are two active donor sites present. As a follow-up to our previous work on compounds based on bis pyrazolone[27-31], here we detail the creation of some brand-new Cu(II) and Ni(II) heterochelates as well as spectroscopic, thermal and biological investigation of these compounds. Fig. 1 depicts the basic shape of the ligands (DPLn).

Experimental Section

All of the compounds were of analytical grade and did not require further purification before usage. The compound diamine diphenyl sulfone (DDS) was obtained from Avra synthesis Pvt. Ltd. while the compound 1(4-nitro) phenyl 3-methyl 5-pyrazolone was supplied by Nutan Dyechem. Pvt Ltd., Sachin, Surat, which was used after recrystallization. Dioxane and acyl chlorides were obtained from Sigma Ltd. (India). Other solvents were used after purifying by standard techniques.

The elements C, H and N were analyzed using a Perkin-Elmer chemical analyzer model 2400. Infrared

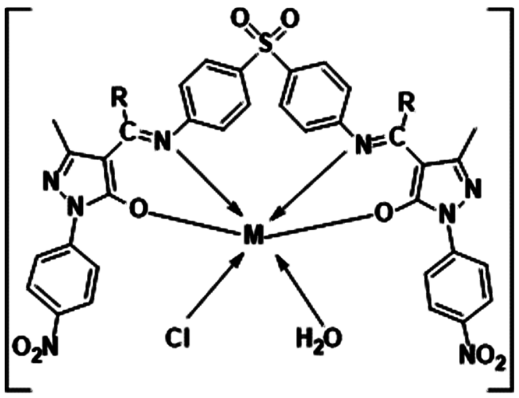

Fig. 1 — Proposed structure of Heterochelate

(IR) spectra were captured using a Perkin Elmer type RX 1 FTIR using KBr pellets. DMSO-d_6 was used as the solvent for recording the ^{1}H NMR spectra and TMS served as the internal reference on a Bruker AV 400 MHz NMR instrument. The mass fragmentation patterns (FAB) of the synthesized compounds were obtained at SAIF CDRI Lucknow. On the EX STAR 6000 TG/DTG 6300 variant, a TG/DTG was logged. DSC was performed at CSIR-CSMCRI-Bhavnagar, using a Universal V3.0 DSC apparatus in the temperature range of 0-1000°C. The trial was conducted in an environment of N_2 at a 10°C/min heating rate.

General procedure for the synthesis of ligands

The synthesis of the Schiff base ligands involved heating a 25 mL methanolic solution of diamine diphenyl sulfone (DDS) (0.01 mol) with 1(4-nitro) phenyl 3-methyl 4-acyl 5-pyrazolone (0.02 mol) for 3 to 4 hours while stirring, adding catalytic amounts of glacial acetic acid and monitoring the reaction's progress with TLC. The solvent was eliminated through evaporation. Yielding a pigmented oily product that was then purified by crystallizing in the proper solvent after being rinsed with diethyl ether and desiccated in vacuum to constant mass.

Physical and Spectral Data of ligands

DPL1: Yield 78%. m.p.292°C. FT-IR (KBr): 3373.50 (O–H), 2926.01 (N–H), 1631.78 (C=O), 1539.20 cm^{-1} (C=N); ^{1}H NMR (400 MHz, DMSO-d_6): δ 2.36-2.42 (6H, s, -2CH_3); 2.43-2.50 (6H, s, 2CH_3) 7.60-8.31; (8H, m, Ar-H); 6.62-7.59; (8H, m, py-H); 12.67-12.79 (2H, s, 2-OH). Anal. $C_{36}H_{30}N_8O_8S$: Calcd Found (%): C, 58.97% (59.1%); H, 4.24% (4.28%); N, 15.32% (15.36%), O, 17.49% (17.53%), S, 4.44% (4.52%).

DPL2: Yield 71%. m.p.325°C. FT-IR (KBr): 3360.00 (O–H), 2926.00 (N–H), 1629.85 (C=O), 1535.14 cm^{-1} (C=N); ^{1}H NMR (400 MHz, DMSO-d_6): δ 2.34-2.43 (6H, s, -2CH_3); 1.12-1.16 (6H, s, 2CH_3); 2.73-2.75 (4H, m, -2CH_2) 6.64-7.97; (8H, m, py-H); 7.5-7.86; (8H, m,Ar-H); 12.63-12.74 (2H;s 2-OH. Anal. $C_{38}H_{34}N_8O_8S$: Calcd Found (%): C, 59.83% (60.42%); H, 4.49% (4.61%); N, 14.69% (14.85%); O, 16.78% (16.95%) S, 4.20% (4.32%).

DPL3: Yield 76%. m.p.351-353°C. FT-IR (KBr): 3116.97 (O–H), 2935.60 (N–H), 1624.06 (C=O), 1533.41 cm^{-1} (C=N): ^{1}H NMR (400 MHz, DMSO-d_6): δ 2.23-2.46 (6H, s, -2CH_3); 0.84-0.86 (6H, t, 2CH_3); 1.58-1.60 (4H, m, -2CH_2); 2.15-2.2 (4H, t, -2CH_2); 6.56-7.26 (8H, m, py-H); 7.29-8.14; (8H, m, Ar-H); 12.63-12.79 (2H, s, 2-OH). Anal. $C_{40}H_{38}N_8O_8S$: Calcd Found (%): C, 60.75% (60.87%); H, 4.84% (4.94%); N, 14.17% (14.23%); O, 16.18% (16.25%); S, 4.05% (4.14%).

DPL4: Yield 63%. m.p.403°C. FT-IR (KBr): 3173.50 (O–H), 2931.80 (N–H), 1622.13 (C=O), 1537.27 cm^{-1} (C=N); ^{1}H NMR (400 MHz, DMSO-d_6): δ 2.22-2.28 (6H, s, -2CH_3), 8.10-8.33 (8H, m, py-H), 7.17-7.89 (10H, m, Ar-H) 7.74-8.09 (8H, m, Ar-H) 12.41-12.46 (2H, s; -OH). Anal. $C_{46}H_{34}N_8O_8S$; Calcd Found (%): C, 64.33% (64.45%); H, 3.99% (4.12%); N, 13.05% (13.18%); O, 14.90% (14.68%); S, 3.73% (3.85%).

DPL5: Yield 59.8%. m.p.489-495°C. FT-IR (KBr): 3120.82 (O–H), 2812.20 (N–H), 1627.92 (C=O), 1502.55 cm^{-1} (C=N) ^{1}H NMR (400 MHz, DMSO-d_6): δ 1.38-1.47 (6H, s, -2CH_3), 6.58-7.12 (8H, m, py-H), 7.14-7.47 (8H, m, Ar-H), 7.49-8.07 (8H, m, Ar-H); 12.48-12.52 (2H, s, -OH). Anal. $C_{46}H_{32}N_{10}O_{12}S$; Calcd Found (%): C, 58.50% (58.65%); H, 3.76% (3.82%); N, 14.52% (14.64%); O, 19.90% (19.98%); S, 3.32% (3.45%).

General procedure for the synthesis of heterochelates

Each heterochelate of the Schiff base was prepared using the basic approach outlined below. A 25 mL methanol solution of the appropriate Schiff base, DPL1 (0.01 mol), DPL2 (0.01 mol), DPL3 (0.01

mol), DPL4 (0.01 mol), or DPL5 (0.01 mol) was added to $CuCl_2.2H_2O$ and $NiCl_2.6H_2O$ (0.01 mol) solutions. After the full addition, the reaction mixture was refluxed for 6-7 hours before being condensed to lose some of its volume. The resulting precipitate was vacuum filtered and desiccated in desiccators.

Physical and Spectral Data of heterochelates

[Cu(DPL1)Cl·H_2O]·$2H_2O$: Mol. Wt. 887.74. Color: Yellow. Yield 72%. FT-IR (KBr): 3226.13 (O–H), 2785.10 (N–H), 1614.42 (C=O), 1510.26 (C=N). Anal. Calcd Found (%): C, 49.20% (48.80%); H, 3.12% (3.80%); Cl, 4.09% (4.00%); N, 13.02% (12.60%); O, 20.02% (19.80%); Cu, 7.21% (7.17%).

[Cu(DPL2)Cl·H_2O]·1.5 H_2O: Mol. Wt. 877.8. Color: Dark yellow. Yield 76%. FT-IR (KBr): 2978.09 (O–H), 2829.50 (N–H), 1618.28 (C=O), 1517.98 (C=N). Anal. Calcd Found (%): C, 52.07% (52.00%); H, 3.14% (3.90%); Cl, 4.07% (4.04%); N, 13.01% (12.70%); O, 16.71% (16.40%); Cu, 7.30% (7.24%).

[Cu(DPL3)Cl·H_2O]Cl·H_2O: Mol. Wt. 959.3. Color: Yellow. Yield 73%. FT-IR (KBr): 3085.16 (O–H), 2826.10 (N–H), 1585.49 (C=O), 1516.04 (C=N). Anal. Calcd Found (%): C, 51.08% (50.00%); H, 4.57% (4.20%); Cl, 7.45% (7.39%); N, 12.02% (11.60%); O, 16.85% (16.68%); Cu, 6.72% (6.60%).

[Cu(DPL4)Cl·H_2O]3Cl·H_2O: Mol. Wt. 1098.25. Color: Light yellow. Yield 67%. FT-IR (KBr): 3263.14 (O–H), 2847.10 (N–H), 1606.70 (C=O), 1508.33 (C=N). Anal. Calcd Found (%): C, 50.90% (50.30%); H, 3.41% (3.30%); Cl, 13.02% (12.90%); N, 10.04% (10.20%); O, 14.69% (14.57%); Cu, 5.78% (5.70%).

[Cu(DPL5)Cl·H_2O]2Cl·H_2O: Mol. Wt. 1152.79. Color: Yellow. Yield 63%. FT-IR (KBr): 3100.03 (O–H), 2785.10 (N–H), 1612.40 (C=O), 1500.62 (C=N). Anal. Calcd Found (%): C, 47.13% (47.9%); H, 3.38% (2.90%); Cl, 9.28% (9.23%); N, 12.80% (12.20%); O, 19.51% (19.43%); Cu, 5.57% (5.50%).

[Ni(DPL1)Cl·H_2O]Cl·$3H_2O$: Mol. Wt. 936.43. Color: Light yellow. Yield 74%. FT-IR (KBr): 3552.88 (O–H), 2823.79 (N–H), 1627.92 (C=O), 1496.76 (C=N). Anal. Calcd Found (%): C, 51.24% (51.18%); H, 4.06% (3.58%); Cl, 4.25% (4.20%); N, 13.33% (13.26%); O, 17.48% (17.40%); Ni, 13.85% (13.20%).

[Ni(DPL2)Cl·H_2O]Cl·$1.5H_2O$: Mol. Wt. 932.44. Color: Yellow. Yield 76%. FT-IR (KBr): 3031.72 (O–H), 2895.31 (N–H), 1629.85 (C=O), 1516.05 (C=N). Anal. Calcd Found (%): C, 52.34% (52.28%); H, 4.01% (3.93%); Cl, 4.09% (4.06%); N, 12.95% (12.84%); O, 17.02% (16.50%); Ni, 6.81% (6.72%).

[Ni(DPL3)Cl·H_2O]Cl·H_2O: Mol. Wt. 954.46. Color: Light green. Yield 71%. FT-IR (KBr): 3105.12 (O–H), 2876.47 (N–H), 1624.06 (C=O), 1516.05 (C=N). Anal. Calcd Found (%): C, 51.02% (50.34%); H, 4.29% (4.22%); Cl, 7.49% (7.43%); N, 11.79% (11.74%); O, 16.80% (16.70%); Ni, 6.21% (6.15%).

[Ni(DPL4)Cl·H_2O]3Cl·H_2O: Mol. Wt. 1091.50. Color: Dark yellow. Yield 68%. FT-IR (KBr): 3195.14 (O–H), 2812.10 (N–H), 1622.13 (C=O), 1510.26 (C=N). Anal. Calcd Found (%): C, 57.11% (57.02%); H, 3.61% (3.54%); Cl, 3.73% (3.66%); N, 11.62% (11.56%); O, 14.91% (14.80%); Ni, 6.14% (6.06%).

[Ni(DPL5)Cl·H_2O]2Cl·H_2O: Mol. Wt. 1149.94. Color: Brown. Yield 65%. FT-IR (KBr): 2995.10 (O–H), 2796.05 (N–H), 1624.06 (C=O), 1502.55 (C=N). Anal. Calcd Found (%): C, 48.22% (48.13%); H, 3.06% (2.99%); Cl, 9.82% (9.77%); N, 12.29% (12.20%); O, 19.65% (19.51%); Ni, 5.23% (5.11%).

Results and Discussion

Elemental analysis, IR, ^{1}H NMR, and mass spectroscopy were utilized to investigate the structural details of all the produced ligands (DPL1-DPL5). Cu(II) and Ni(II) chloride were combined in a 1:1 ratio with a range of ligands (DPL1-DPL5) to create the heterochelates.

IR Spectra

The Infrared spectra of Schiff base (DPL1 to DPL5) were equated with spectra of the matching heterochelate reported in experimental section. In order to explore the binding manner of Schiff base (DPL1 to DPL5) to the Cu(II) and Ni(II) ion in the heterochelate. This study's Schiff base ligands display a broad band in the range of 3116.97 to 3373.50 cm^{-1}, which suggests that the -OH group at 5th position is involved in intramolecular H-bonding[32-35]. The lone pair of azomethine further suggests that the ligand exists as an enol in solid form. The acyclic azomethine group of the Schiff base ligand

(DPL1 to DPL5) exhibits a crisp and intense band in the range of 1502.55 to 1539.20 cm^{-1}. The modest energy shift of this band has suggested that azomethine nitrogen is coordinated, which is present in the heterochelate and appears at 1496.76 to 1517.98 cm^{-1} (Ref. 36,37). The IR spectrum of heterochelate exhibits a significant negative shift of 15-20 cm^{-1} in the pyrazolone group's (C=O) absorption, demonstrating that coordination through the oxygen atom of the ligand causes a decrease in the stretching force constant of (C=O). Two novel bands were discovered in the far-IR region, which were attributed to the ν(M-O) pyrazolone and (M-O) ketone of the ligand modes correspondingly in the complexes. These bands were found at 442-476 and 414-434 cm^{-1}. All of this information demonstrates that (DPL1 to DPL5) act as dinegative bidentate ligands and form conjugate chelate rings by ligands that are already present in heterochelates in the enolic state.

^{1}H NMR Spectra

There have been a lot of investigations done on the tautomerism of pyrazolone[38]. In DMSO-d_6 at normal temperature, Schiff base ligand ^{1}H NMR investigations were conducted. In the instance of two sharp singlets that correspond to one and two protons were seen in the range of 12–13 ppm which corresponds to the -OH group in the ligand's ^{1}H NMR spectra and the data are represented in the investigational section. In the course of a D_2O exchange experiment, this signal vanished. Signals for methyl groups in Schiff base ligands are seen in the range of 2.0 to 2.8 ppm, and aromatic protons are seen in the range of 7.5 to 8.5 ppm. From the NMR spectra of DPL1 it is observed that all of the signals from the -CH_3, aromatic protons and -OH group[39] in NMR, which are all repeated in a particular order, may demonstrate the existence of both the keto and enol forms. Additionally, specifying the percentage ratio of each form present in the solution at the time of the analysis may benefit from knowing the signal's strength. As all of these signals are tightly spaced apart and may overlap with either the solvent or moisture peak, it can be challenging to definitively attribute each signal to a specific methyl group[40]. The Keto-Enol form of the Schiff base ligand is found in solution state based on ^{1}H NMR spectroscopic data.

FAB Mass Spectra

[Cu(DPL1)Cl·H_2O]·$2H_2O$

The molecular ion peak and recorded FAB mass band for heterochelate [Cu(DPL1)Cl·H_2O]·$2H_2O$ made clear how the molecule was put together. You can see the intended fragmentation pattern in Scheme 1. The initial peak, m/z=888, is where heterochelates' molecular ion peak may be found. The anticipated fragmentation path of the examined heterochelates is depicted in Scheme 1. Species **(b)**, which has a peak at m/z=799, is produced when species **(a)**, which had coordinated H_2O and Cl molecules, loses these molecules. This is the main reason for the fragmentation of the heterochelate. By continuing to degrade, species **(c)** with missing $C_{12}H_{10}N_4O_3$ are created. When species **(c)** loses $C_{12}H_9O_2S$, it transforms into species **(d)** and when species **(d)** loses CuO, it continues to deteriorate further into species **(e)**. The stable species **(b)** with a 94.0% abundance is represented by the severe peak (base peak) seen at m/z=799 in the spectrum. All of the indicated degradation stages' measured molecular weights were within the predicted range[41].

[Ni(DPL1)Cl·H_2O]·Cl·$3H_2O$

The molecular ion peak for the heterochelate [Ni(DPL1)Cl·H_2O]Cl·$3H_2O$ and the recorded FAB mass spectra has been utilised to validate the molecular composition of [Ni(DPL1) Cl·H_2O] Cl·$3H_2O$. As demonstrated in Fig. 2 and with its disintegration form provided in Scheme 2, exhibits a

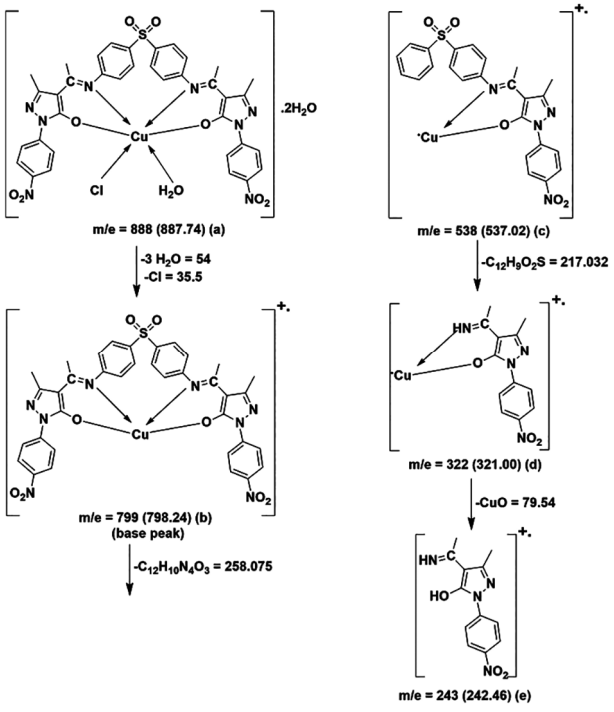

Scheme 1 — Suggested fragmentation pattern for [Cu(DPL1) Cl·H_2O]·$2H_2O$ mass spectra

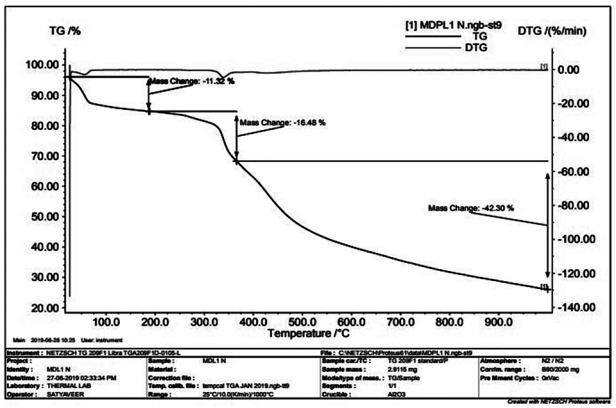

Fig. 2 — TG/DTG Curve of Heterochelate [Ni(DPL1) $Cl{\cdot}H_2O]{\cdot}Cl{\cdot}3H_2O$

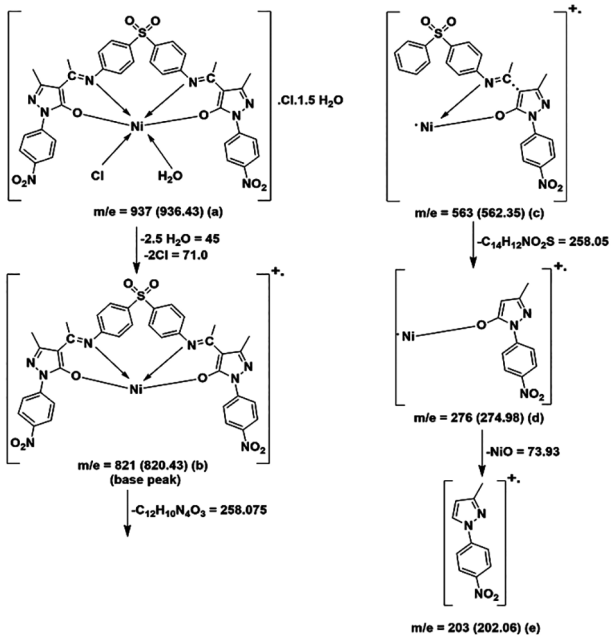

Scheme 2 — Suggested fragmentation pattern for [Ni(DPL1) $Cl{\cdot}H_2O]{\cdot}Cl{\cdot}3H_2O$ mass spectra

significant number of peaks that correlate to the molecule's progressive fragmentation. The heterochelate's molecular ion peak is shown by the first peak at m/e=937. The loss of three H_2O and one Cl molecule from species **(a)** results in the basic destruction of the heterochelate, which produces species **(b)**, It has an abundance of 93% and a base peak at m/e=821. The loss of $C_{12}H_{10}N_4O_3$ results in species **(c)** after additional degradation. With the loss of $C_{14}H_{12}NO_2S$, species **(c)** progressively deteriorate into species **(d)**. As species **(d)** transitions into species **(e)**, NiO residue is left behind.

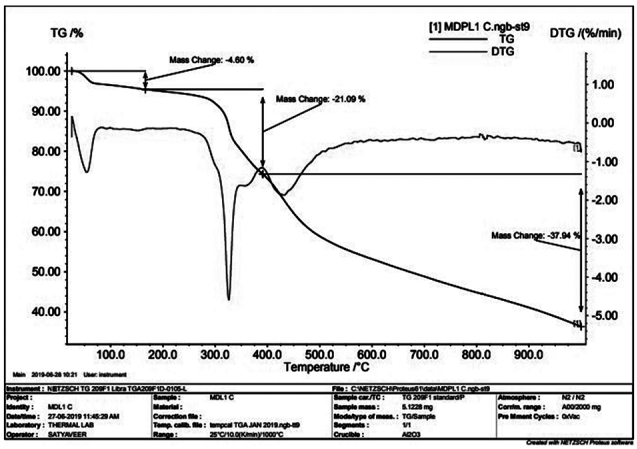

Fig. 3 — TG/DTG Curve of Heterochelate [Cu(DPL1) $Cl{\cdot}H_2O]{\cdot}2H_2O$

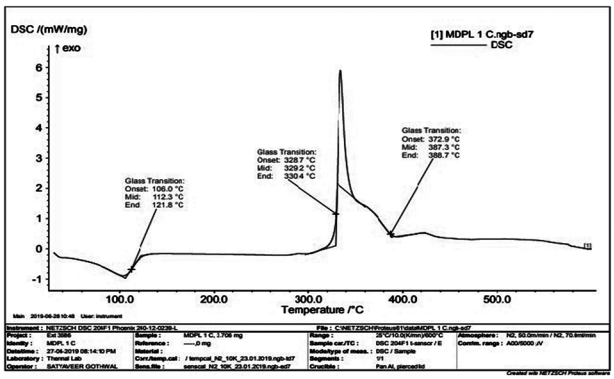

Fig. 4 — DSC Curve of Heterochelate [Cu(DPL1)$Cl{\cdot}H_2O]{\cdot}2H_2O$

Thermal Response of Synthesized Heterochelate

Every decomposition procedure complies with the trend.

Solid-1 degrade to gives Solid-2 + Gas

This procedure is divided into numerous steps:

$[Cu(DPLn){\cdot}Cl{\cdot}H_2O]{\cdot}xH_2O{\cdot}yCl$

TGA curve of heterochelate [Cu(DPL1) $Cl{\cdot}H_2O]{\cdot}2H_2O$ is signified in Fig. 3. The decay of heterochelate [Cu(DPL1)$Cl{\cdot}H_2O]{\cdot}2H_2O$ occurs in three stages. This heterochelate goes through a single phase of thermal dehydration and dehalogenation between 50 and 165°C a decrease in mass of 4.60% (4.54%). At this step, 2 mol of coordinated H_2O molecules may be removed. At 112.3°C and 121.8°C, respectively, endothermic effects are present along with this process. The second stage, which takes place between 166-395°C, relates to the breakdown of $Cl{\cdot}H_2O$ and a portion of the DPL1 ligand. Mass loss was seen to be 21.90% (21.03%). The DSC curve in Fig. 4 represents the endothermic peak at 388.7°C,

Table 1 — Thermoanalytical data of heterochelates

S. No	Heterochelates	Temp. Range	Mass Loss (%) Obsd (Calcd)	Analysis
1	[Cu(DPL1)Cl·H_2O]·2H_2O	50-165	4.60 (4.54)	Two crystalline water molecule may loss
		166-395	21.09 (21.03)	Cl·H_2O Coordinated molecule and some part of ligand may loss
		396-950	37.94 (37.91)	Remaining Cu may present as CuO
2	[Cu(DPL2)Cl·H_2O]·1.5H_2O	50-215	3.03 (2.97)	1.5H_2O crystalline molecule may loss
		216-405	24.15 (24.04)	Cl·H_2O Co-ordinated molecule and some part of ligand may loss
		406-963	38.13 (38.02)	Leaving CuO residue
3	[Cu(DPL3)Cl·H_2O]·Cl·H_2O	50-278	5.64 (5.56)	Cl·H_2O crystalline molecule may loss
		279-453	26.23 (26.12)	Cl·H_2O Co-ordinated molecule and some part of ligand may loss
		454-969	35.89 (35.77)	Leaving CuO residue
4	[Cu(DPL4)Cl·H_2O]·3Cl·H_2O	50-314	11.35 (11.31)	Crystalline 3Cl and H_2O molecule may loss
		315-525	23.19 (23.12)	Cl·H_2O Co-ordinated molecule and some part of ligand may loss
		526-979	33.17 (33.11)	Leaving CuO residue
5	[Cu(DPL5)Cl·H_2O]·2Cl·H_2O	50-321	7.83 (7.78)	Crystalline 2Cl and H_2O molecule may loss
		322-527	22.18 (22.11)	Cl·H_2O Co-ordinated molecule and some part of ligand may loss
		528-983	48.13 (38.09)	Leaving CuO residue
6	[Ni(DPL1) Cl·H_2O]·Cl·3H_2O	50-190	11.32 (11.24)	3H_2O & Cl crystalline molecule may loss
		191-387	16.48 (16.40)	Cl·H_2 O Co-ordinated molecule and some part of ligand may loss
		388-970	42.30 (42.21)	Remaining Ni may present as NiO
7	[Ni(DPL2)Cl·H_2O]·Cl·1.5H_2 O	50-210	11.42 (11.35)	1.5H_2O crystalline molecule may loss
		211-407	16.71 (16.59)	Cl·H_2O Co-ordinated molecule and some part of ligand may loss
		408-972	42.96 (42.84)	Leaving NiO residue
8	[Ni(DPL3) Cl·H_2O]·Cl·H_2O	50-212	10.93 (10.84)	Cl·H_2O crystalline molecule may loss
		213-413	17.36 (17.21)	Cl·H_2O Co-ordinated molecule and some part of ligand may loss
		414-975	43.24 (43.12)	Leaving NiO residue
9	[Ni(DPL4) Cl·H_2O]·3Cl·H_2O	50-238	11.43 (11.32)	Crystalline 3Cl and H_2O molecule may loss
		239-476	18.23 (18.10)	Cl·H_2O Co-ordinated molecule and some part of ligand may loss
		477-980	44.13 (44.05)	Leaving NiO residue
10	[Ni(DPL5) Cl·H_2O]·2Cl·H_2O	50-242	11.52 (11.40)	Crystalline 2Cl and H_2O molecule may loss
		243-487	18.33 (18.22)	Cl·H_2O Co-ordinated molecule and some part of ligand may loss
		488-982	44.25 (44.13)	Leaving NiO residue

which resembles to this stage. The third stage involves the estimated amount of CuO decomposing at temperatures between 396 and 950°C while experiencing a mass loss of 37.94% (37.91%). Compared to a theoretical value of 63.48%, the overall mass loss that has been measured is 64.49%. According to the discussion above, Fig. 1 depicts the heterochelate's suggested octahedral structure, and Table 1 lists its thermodynamic information.

[Ni(DPLn)·Cl·H_2O]·xH_2O·yCl

TGA curve of heterochelate [Ni(DPL1) Cl·H_2O]·Cl·3H_2O are denoted in Fig. 2 and DSC curve of heterochelate are denoted in Fig. 5. The decomposition of heterochelate [Ni(DPL1) Cl·H_2O]·Cl·3H_2O takes place in three stage. This heterochelate is thermally dehydrated and de-halogenated in a single step between 50 and 190°C with a mass loss of 11.32% (11.24%). At this step, 3 mol of coordinated H_2O and Cl molecules might be eliminated. At 128.4°C and 334.9°C, respectively, an endothermic effect is present throughout this process. The second stage, which takes place in the 191°C to 387°C temperature range, refers to the breakdown of a portion of the DPL_1 ligand. Mass loss was seen to be 16.48% (16.40%). The DSC curve indicates that the endothermic

peak at 392.4°C resembles to this stage. The third stage involves the breakdown of the DPL1 ligand's associated portion and an estimated amount of NiO (Ref. 42) at temperatures between 388 and 970°C, along with a mass loss of 42.30% (42.21%). The observed total mass loss is 69.85%, compared to the predicted figure of 66.32%. According to the discussion above, Fig. 1 depicts the heterochelate's suggested octahedral structure and Table 1 lists its thermodynamic information.

Antimicrobial Screening

Zone of Inhibition

The result concerning antibacterial activity (Zone of Inhibition) of the ligands and their heterochelate are described in Table 2. Every ligand containing heteroatoms has some antibacterial activity[43]. The antibacterial efficacy of the ligands and their heterochelates against *Bacillus cerus*, *Bacillus megaterium*, *E. coli*, and *E. aerogen* was studied and it was discovered that the synthesised heterochelate (CuDPL3) was more effective against *E. coli* than the ligands (DPL3) of Cu and Ni. While the synthetic ligand DPL5 and its heterochelate (NiDPL5) were found to be more effective against *E. coli* in the case of the Ni-complex. All of the complexes were shown to be stronger bactericides than the ligands. The ability of coordination at the metal centre appears to control the inhibitory activity to some extent. Further research on these complexes is suggested by the high antibacterial efficacy of these complexes against tested species. Fig. 6 depicts the ligand and Cu(II) combination's zone of inhibition (mm), while Fig. 7 depicts the Ni(II) complex.

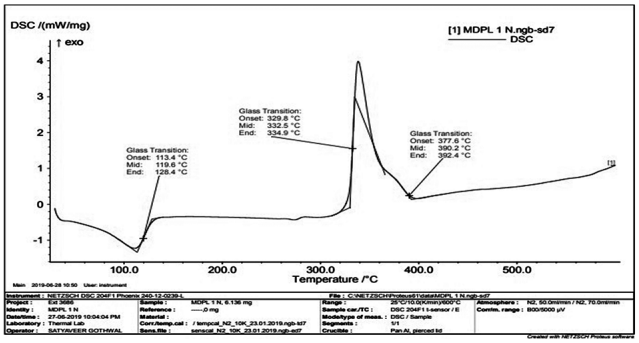

Fig. 5 — SC Curve of Heterochelate $[Ni(DPL1)Cl{\cdot}H_2O]{\cdot}Cl{\cdot}3H_2O$

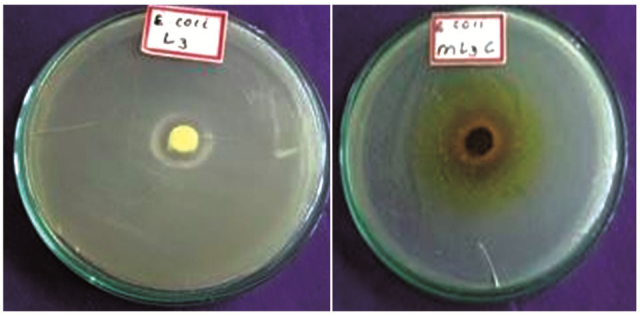

Fig. 6 — Zone of inhibition (mm) of Ligand and Cu(II) Complex

MIC Study

Strong activity against two Gram negative bacteria were shown by the complexes (*Escherichia coli*, *Serratia marcescens*). Table 3 provides information on the compounds' antibacterial properties. The complexes had greater antibacterial activity than free ligands, according to comparative research. Comparing the complexes to the common antibiotic ciprofloxacin, some

Table 2 — Antimicrobial effect data of the ligands and heterochelates

S. No.	Compd	Gram +ve		Gram –ve	
		Bacillus Cerus	*Bacillus Megaterium*	*E.Coli*	*E.Aerogen*
1	DPL1	5	4	7	5
2	DPL2	7	5	10	6
3	DPL3	4	6	10	6
4	DPL4	8	8	8	7
5	DPL5	8	8	6	6
6	$[Cu(DPL1)Cl{\cdot}H_2O]{\cdot}2H_2O$	12	19	13	13
7	$[Cu(DPL2)Cl{\cdot}H_2O]{\cdot}1.5H_2O$	13	16	14	11
8	$[Cu(DPL3)Cl{\cdot}H_2O]{\cdot}Cl{\cdot}H_2O$	15	19	16	10
9	$[Cu(DPL4)Cl{\cdot}H_2O]{\cdot}3Cl{\cdot}H_2O$	14	14	10	14
10	$[Cu(DPL5)Cl{\cdot}H_2O]{\cdot}2Cl{\cdot}H_2O$	17	17	12	11
11	$[Ni(DPL1)Cl{\cdot}H_2O]{\cdot}Cl{\cdot}3H_2O$	12	19	13	13
12	$[Ni(DPL2)Cl{\cdot}H_2O]{\cdot}Cl{\cdot}1.5H_2O$	13	16	14	11
13	$[Ni(DPL3)Cl{\cdot}H_2O]{\cdot}Cl{\cdot}H_2O$	15	19	16	10
14	$[Ni(DPL4)Cl{\cdot}H_2O]{\cdot}3Cl{\cdot}H_2O$	14	14	10	14
15	$[Ni(DPL5)Cl{\cdot}H_2O]{\cdot}2Cl{\cdot}H_2O$	17	17	12	11

of them showed only moderate activity. Moreover, several of the complexes were shown to be stronger bactericides than the ligands. According to Overtone's idea, Tweedy's chelation theory, and the restricted sharing of metal ions' positive charge with donor groups[44] this increase in antibacterial activity is explicable. This could support the theory that various types of bimolecular binding to metal ions, intercalation, or electrostatic contact impede biological synthesis and prevent organisms from reproducing. According to the findings of our research, compounds [Cu(DPL1)Cl·H_2O]·$2H_2O$ and [Ni(DPL3)Cl·H_2O]·Cl·H_2O are effective against Staphylococcus aureus, whereas [Cu(DPL2)Cl·H_2O]·$1.5H_2O$ and [Ni(DPL3)Cl·H_2O]·Cl·H_2O are effective against *Escherichia coli* and have high affinity for most receptors. These chemicals should be further researched due to their potent antibacterial effects on the examined species.

Strong antimicrobial effects are shown by the Cu(II) and Ni(II) complexes against the Gram(+ve) and Gram(–ve) pathogens *Staphylococcus aureus* and *Bacillus subtilis*, respectively. Table 3 shows the MIC results for the ligands and their complexes' *in vitro* antibacterial activity. When compared to metal salts and ligands, all of the complexes have significantly greater antibacterial activity against the four pathogens, and when compared to ofloxacin, all of the complexes were found to have stronger bacteriostatic properties than the ligands. Cellular permeability has increased, which is the reason of this. Only lipid-soluble substances may pass through the lipid membrane that encircles the cell, and it is well recognised that liposolubility is a key determinant of antimicrobial action. Overtone's notion and Tweedy's chelation theory[45] suggest a possible way for increasing biocidal action. According to this, chelation diminishes the polarity of the central atom primarily through partial sharing of its positive charge with donor groups and probable electron delocalization within the chelation ring. This increases the lipophilic character of the core manganese atom, which favours its penetration through the cell membrane's lipid layer. Our research findings According to Table 3, the molecules [Cu(DPL1)Cl·H_2O]·$2H_2O$ and [Ni(DPL3)Cl·H_2O]·Cl·H_2O have good action against Staphylococcus aureus and [Ni(DPL1)Cl·H_2O]·Cl·$3H_2O$ having good activity against *Bacillus subtilis*, while [Cu(DPL3)Cl·H_2O]·Cl·H_2O and [Ni(DPL2)Cl·H_2O]·Cl·$1.5H_2O$ have good activity against *Escherichia coli* with high affinities to most receptors. The high antibacterial activity of these compounds against tested pathogens warrant further investigation.

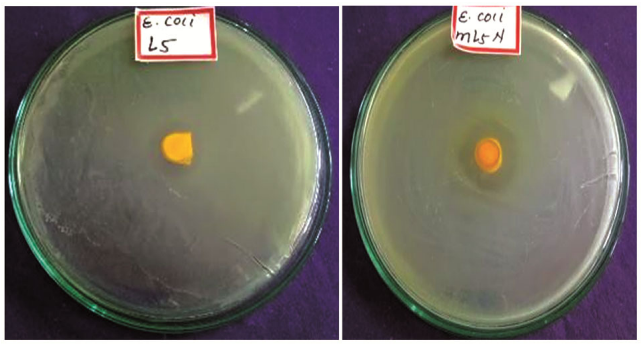

Fig. 7 — Zone of inhibition (mm) of Ligand and Ni(II) complex

Table 3 — Minimum inhibitory concentrations (ppm) data of the compounds against bacteria

S. No.	Compd	Gram +ve		Gram –ve	
		Staphylococcus aureus	*Bacillus Subtilis*	*Escherichia coli*	*Serratia marcescens*
1	Ofloxacin	0.6	0.5	0.6	0.7
2	$CuCl_2·2H_2O$	150	250	300	350
3	$NiCl_2·6H_2O$	250	200	350	400
4	DPL1	105	115	130	105
5	DPL2	110	115	120	115
6	DPL3	110	120	125	110
7	DPL4	100	110	120	120
8	DPL5	105	115	125	135
9	[Cu(DPL1)Cl·H_2O]·$2H_2O$	0.5	1.2	0.9	1.0
10	[Cu(DPL2)Cl·H_2O]·$1.5H_2O$	0.8	0.6	1.0	1.1
11	[Cu(DPL3)Cl·H_2O]·Cl·H_2O	1.2	0.7	0.25	0.5
12	[Cu(DPL4)Cl·H_2O]·3Cl·H_2O	1.6	0.9	1.2	1.0
13	[Cu(DPL5)Cl·H_2O]·2Cl·H_2O	2.0	1.8	1.9	1.6
14	[Ni(DPL1)Cl·H_2O]·Cl·$3H_2O$	1.2	0.35	1.2	1.8
15	[Ni(DPL2)Cl·H_2O]·Cl·$1.5H_2O$	0.8	1.1	0.42	0.9
16	[Ni(DPL3)Cl·H_2O]·Cl·H_2O	0.56	1.9	1.7	0.8
17	[Ni(DPL4)Cl·H_2O]·3Cl·H_2O	1.7	1.0	0.6	1.4
18	[Ni(DPL5)Cl·H_2O]·2Cl·H_2O	1.1	1.3	0.9	0.95

Conclusion

In the current work, the synthesis, characterisation, and Cu(II) and Ni(II) complexes of novel 4 acyl pyrazolone-based bis pyrazolone ligands were described. Studies using the ^{1}H NMR, FT-IR, and mass spectrometers showed that the ligand can exist as a tautomeric enol in both the solid and solution states with intramolecular H-bonding. A tentative structure for metal(II) heterochelates is presented in Fig. 1 based on the results of spectroscopic and thermal analyses. For bioactivity, all of the produced substances were tested. The heterochelates displayed potent antimicrobial effects. According to the data, Cu(ll) and Ni(II) complexes may be able to sustain strong antibacterial effects and function as a potent, broad-spectrum antibiotic that may be able to address some antibacterial resistance issues.

Supplementary Information

Supplementary information is available in the website http://nopr.niscpr.res.in/handle/123456789/58776. The supplementary information includes ^{1}H NMR spectrum of ligand DPL1 and FAB mass spectrum of heterochelates $[Cu(DPL1)Cl\cdot H_2O]\cdot 2H_2O$ and $[Ni(DPL1)Cl\cdot H_2O]\cdot Cl\cdot 3H_2O$ respectively.

References

1 Yang Z Y, Yang R D, Li F S & Yu K B, *Polyhedron*, 19 (2000) 2599.
2 Poormohammadi E B, Behzad M, Abbasi Z & Astaneh S D A, *J Mole Struc*, 1205 (2020) 127603.
3 Shaikh I, Jadeja R N, Patel R, Mevada V & Gupta V K, *J Mole Struc*, 1232 (2021) 130051.
4 Shaikh I, Jadeja R N & Patel R, *Polyhedron*, 183 (2020) 114528.
5 Luo H Y, Li J Y, Li Y, Zhang L, Li J Y, Jia, D Z & Xu G C, *RSC advances*, 6 (2016) 114997.
6 Shaikh I, Vohra A, Devkar R & Jadeja R, *Eur J Chem*, 10 (2019) 131.
7 Vyas K M, Jadeja R N, Patel D, Devkar R V & Gupta V K, *Polyhedron*, 80 (2014) 20.
8 Wang J, Xu G C, Zhang Y P, Luo H Y, Li J Y, Zhang L & Jia D Z, *New J Chem*, 43 (2019) 2529.
9 Shaabani B, Kh&ar A A, Dusek M, Pojarova M & Mahmoudi F, *Inorganica Chimica Acta*, 394 (2013) 563.
10 Casas J S, Garcia-Tasende M S, Sanchez A, Sordo J & Touceda A, *Coord Chem Rev*, 251 (2007) 1561.
11 Raman N, Kulandaisamy A, Shunmugasundaram A & Jeyasubramanian K, *Transition Metal Chem*, 26 (2001) 131.
12 Uzoukwu B A, Adiukwu P U, Al-Juaid S S, Hitchcock P B & Smith J D, *Inorganica Chimica Acta*, 250 (1996) 173.
13 Yang Z Y, Yang R D, Li F S & Yu K B, *Polyhedron*, 19 (2000) 2599.
14 Wei-fan Y, Shuanggui Y, Yanbing X, Yonghou X, Ke-ming F & Bing X, *J Radioanal & Nuc Chem*, 256 (2003) 149.
15 Chiba P, Holzer W, Landau M, Bechmann G, Lorenz K, Plagens B & Ecker G, *J Med Chem*, 41 (1998) 4001.
16 Marchetti F, Pettinari C, Di Nicola C, Tombesi A & Pettinari R, *Coord Chem Rev*, 401 (2019) 213069.
17 Kalarani N, Sangeetha S, Kamalakannan P & Venkappayya D, *Russian J Coord Chem*, 29 (2003) 845.
18 Yoshikuni T, *J Mol Cat A: Chem*, 148 (1999) 285.
19 Marchetti F, Pettinari C, Pettinari R, Cingolani A, Leonesi D & Lorenzotti A, *Polyhedron*, 18 (1999) 3041.
20 Marchetti F, Pettinari C & Pettinari R, *Coord Chem Rev*, 249 (2005) 2909.
21 Casas J S, Garcia-Tasende M S, Sanchez A, Sordo J & Touceda A, *Coord Chem Rev*, 251 (2007) 1561.
22 Pettinari C, Marchetti F, Drozdov A, Vertlib V & Troyanov S, *Inorg Chem Comm*, 4 (2001) 290.
23 Yang L & Yang R, *Polyhedron*, 14 (1995) 507.
24 Li X & Yang R, *Polyhedron*, 11 (1992) 1545.
25 Keter F K & Darkwa J, *Biometals*, 25 (2012) 9.
26 Jani D H, Patel H S, Keharia H & Modi C K, *Applied Organomet Chem*, 24 (2010) 99.
27 Modi C K & Jani D H, *Applied Organomet Chem*, 25 (2011) 429.
28 Raja M N, Jani D H & Koradiya S B, *JETIR*, 6 (2019) 784.
29 Raja M N, Jani D H, *JETIR*, 6 (2019) 641.
30 Somaiya C P, Patel D S & Jani D H, *J Applicable Chemistry*, 8 (2019) 1135.
31 Modi C K & Thaker B T, *J Thermal Anal & Calor*, 94 (2008) 567.
32 Surati K R & Thaker B T, *J Coord Chem*, 59 (2006) 1191.
33 Marchetti F, Pettinari C, Cingolani A, Pettinari R, Rossi M & Caruso F, *J Organomet Chem*, 645 (2002) 134.
34 Marchetti F, Pettinari C, Pettinari R, Cingolani A, Leonesi D & Lorenzotti A, *Polyhedron*, 18 (1999) 3041.
35 Xu G, Liu L, Zhang L, Liu G, Jia D & Lang J, *Structural Chem*, 16 (2005) 431.
36 Akama Y & Tong A, *Microchem J*, 53 (1996) 34.
37 Alafandy M, Willem R, Mahieu B, Alturky M, Gielen M, Biesemans M & Kauffmann J M, *Inorganica Chimica Acta*, 255 (1997) 175.
38 Jadeja R N & Shah J R, *Polyhedron*, 26 (2007) 1677.
39 Patel S H, Pansuriya P B, Chhasatia M R, Parekh H M & Patel M N, *J Thermal Anal & Calor*, 91 (2008) 413.
40 Chohan Z H, *Applied Organomet Chem*, 16 (2002) 17.
41 Dharmaraj N, Viswanathamurthi P & Natarajan K, *Trans Metal Chem*, 26 (2001) 105.
42 Zawadzińska K, Gostyński B, *Scientiae Radices,* 2 (2023) 25.
43 Chohan Z H, Khan K M & Supuran C T, *Applied Organomet Chem*, 18 (2004) 305.
44 Panchal P K, Parekh H M, Pansuriya P B & Patel M N, *J Enzyme Inhib & Med Chem*, 21 (2006) 203.
45 Tweedy B G, *Phytopathology*, 55 (1964) 910.